HYDROLOGICAL PROCESSES
Hydrol. Process. **28**, 1358–1371 (2014)
Published online 14 January 2013 in Wiley Online Library
(wileyonlinelibrary.com) DOI: 10.1002/hyp.9655

Influence of inclination and permeability of solitary woody riparian plants on local hydraulic and sedimentary processes

Thomas Euler,[1]* Julian Zemke,[2] Stéphane Rodrigues[3] and Jürgen Herget[4]

[1] *Hydrotec, Ingenieurgesellschaft für Wasser und Umwelt mbH Bachstr. 62-64 52066 Aachen, Germany*
[2] *University of Koblenz-Landau, Department of Geography, Koblenz, Germany*
[3] *GéoHydrosystèmes Continentaux, EA 6293 GéHCO Université François Rabelais de Tours, Faculté des Sciences et TechniquesParc de Grandmont, F-37200 Tours, France*
[4] *University of Bonn Department of Geography Bonn, Germany*

Abstract:

The role of solitary woody riparian plants with respect to local erosion and deposition of sediments is investigated. A focus is laid on the characteristics 'inclination' and 'permeability' of the plant's projected frontal area. Therefore, two experimental studies using cylindrical obstacles were carried out in a laboratory flume, one aiming at inclination, the other at permeability. The first series revealed that the total amount of mobilized sediment around the cylinder on average decreased by 8–10% per 5° increasing inclination in streamwise direction. Locations of maximum scour depth simultaneously shifted downstream. A horseshoe vortex system, causing the frontal and lateral scouring, ceased to exist below inclinations of 25–30°. The second series revealed that with increasing permeability, frontal scour incision is delayed, and the eroded sediment volume is significantly reduced. With permeable obstacles, two system states were observed: first, frontal scouring with leeside deposition at higher flow velocities and, second, moderate leeside scouring at lower flow velocities. For up-scaling and comparison, a field study focussing on fluvial obstacle marks at poplars and willows in secondary channels of the River Loire was additionally conducted. A modified analytical model enabled us to quantify the amount of deposited sediments leeside of the plants. Leeside sediment ridges are significantly stabilized and have a higher preservation potential when covered by pioneer vegetation. Under such conditions, they may indeed induce the development of stable islands. Eventually, 'sediment ridge width' turned out to be a suitable indicator for leeside deposited sediment volume, irrespective of spatial scale. Copyright © 2012 John Wiley & Sons, Ltd.

KEY WORDS obstacle mark; island formation; ecosystem engineer; riparian vegetation; biogeomorphology; ecohydraulics

Received 24 February 2012; Accepted 20 November 2012

INTRODUCTION

The abundance and spatial extension of riparian plants has significant influence on fluvial landform dynamics and river patterns (e.g. Hupp & Osterkamp, 1996; Francis, 2006; Corenblit *et al*., 2007; Tal & Paola, 2010; Paola, 2011, Gibling & Davies, 2012). In fluvial environments, plants can act as ecosystem engineers by altering sediment fluxes and current stresses to their benefit. They thereby directly influence the availability of resources for other organisms (Gurnell & Petts, 2004; Francis, 2006). However, up to now, little attention has been drawn to the local interactions of hydraulics, sedimentary processes, and plant characteristics at the individual tree or shrub scale (Schnauder & Moggridge, 2009). This work hence aims at investigating mechanical characteristics of solitary trees and shrubs and their effect on local water and sediment movement.

Examples from field studies illustrate that under flood exposure, trees and shrubs induce the leeside deposition of sediments (Osterkamp & Costa, 1987; Baker & Kochel, 1988; Nanson & Knighton, 1996; Fielding *et al*., 1997; Osterkamp, 1998; Tooth & Nanson, 2000; Nakayama *et al*., 2002; Tanaka & Yagisawa, 2010; Corenblit *et al*., 2011; Gurnell *et al*., 2012). The leeside accumulated sediments are partially finer than those of the surrounding streambed, leading to a locally increased field capacity and favouring a nutrient-rich substrate (Gurnell & Petts, 2004). For example, Tanaka and Yagisawa (2010) have measured that the D_{50} value of sediment accumulation leewise of *Salix* and *Robinia* plants in the Arakawa River (Japan) was, on average, 50–80% finer than upstream of the plants (with D_{50} = median particle diameter). This precondition promotes the colonization of both herbs and other woody species, which in turn stabilizes the deposited sediment (Gurnell & Petts, 2004; Rodrigues *et al*., 2007), eventually leading to island development and sometimes – in the long-term – even to channel bifurcation (Nanson & Knighton, 1996; Tooth & Nanson, 2000).

Trees with single straight trunks can also induce frontal scouring (in Baker & Kochel, 1988; Figure 1b), a phenomenon often occurring at bridge-piers (Melville & Coleman, 2000). Because of pressure gradients arising at the trunk, the approaching flow is then forced to move downwards, leading to initial scouring of the streambed. Thereupon, a horseshoe vortex emerges that causes further incision of the scour hole (Unger & Hager, 2007). After being removed by the horseshoe vortex, the grains are

*Correspondence to: Thomas Euler, Hydrotec, Ingenieurgesellschaft für Wasser und Umwelt mbH Bachstr. 62-64 52066 Aachen, Germany.
E-mail: t-euler@gmx.de

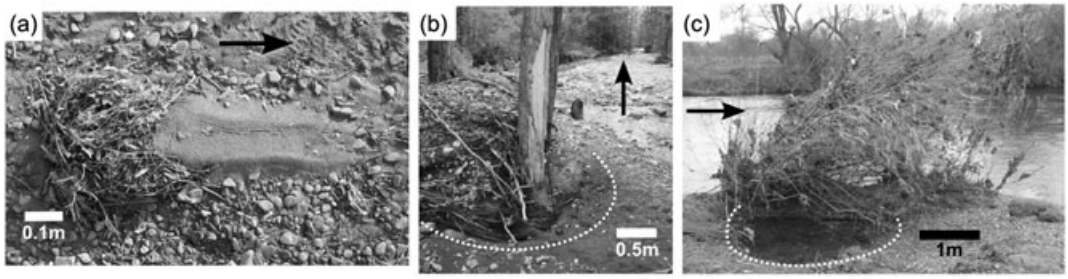

Figure 1. (a) Accumulation of medium sand leeside of a shrub in a gravelly secondary channel of the Sieg River (Germany); (b) local scouring (dotted line) and erosional scars in front of a coniferous tree after a flash flood in the Miette River (Canada); (c) lateral scouring (dotted line) at a significantly inclined willow growing near the bank of the Sieg River. The white dotted lines indicate local scouring

transported out of the scour hole and deposited leeside of the tree in a tapered arrangement because of the action of wake vortices (Euler & Herget, 2012). For a cylindrical obstacle, the amount of locally scoured and deposited material basically increases with increasing size of the projected frontal area of the obstacle, with increasing approaching flow velocity and with an increasing ratio between obstacle diameter and median grain size of the sediments (Euler & Herget, 2011; Euler & Herget, 2012). In fluvial geomorphology, forms consisting of a frontal scour hole in combination with tapered leeside sediment accumulation around an obstacle are denoted as 'obstacle marks' (Karcz, 1968; Allen, 1984). The formation of fluvial obstacle marks is a non-linear mechanism, controlled by feedback loops between hydraulic and sedimentary processes (Euler, 2012). In the worst case, however, local scouring can lead to root excavation and tree removal by the current under flood waves as Rominger *et al.* (2010) demonstrated in a large-scale experiment, and Fielding *et al.* (1997) have reported from a field study. Woody riparian plants appear to have developed 'autogenic' (Francis, 2006) mechanical characteristics that reduce the probability of root excavation, while promoting leeside sediment deposition for creation of new micro-habitats. These local scale variations in biogeomorphic influence affect the likelihood of pioneer island formation. Thus, a basic understanding of the involved fine-scale processes is necessary to explain the emergence of related larger-scale river patterns. In this context, there are two major mechanical characteristics of solitary riparian plants that play an important role but whose influences on sedimentary structures have not been investigated systematically yet: 'Trunk/plant inclination in streamwise direction' and 'permeability of the plant body'.

Inclination

Nakayama *et al.* (2002) report that *Melaleuca argentea* trees growing on bars of the Burdekin river in north-Queensland (Australia) are inclined in the downstream direction by 15–40° (with 90° being perpendicular to the flumebed, i.e. vertical) and show sediment tail domination, i.e. net deposition of sediments and minor frontal scouring. Tooth & Nanson (2000) have documented that the ability of tea-trees (*Melaleuca glomerata*) to incline into the streamwise direction when exposed to flood flows induces the formation of stable islands that are colonized by juvenile tea trees. Many tree species growing in the riparian zone, such as *Salicacea* plants, have flexible stems and/or a high bending ability (Karrenberg *et al.*, 2002) to withstand flood stress and to prevent uprooting (Fielding *et al.*, 1997; Figure 1c). Under permanent exposure to fluid flow during their lifespan trees even feature permanently inclined trunks. When inclined in flow direction, the amount of downflow and deflected energy in front of the obstacle decreases, because of a reduction of the pressure gradient acting at the projected frontal area (Fielding *et al.*, 1997). This also diminishes the power of the horseshoe vortex and, thus, reduces frontal scouring, while promoting lateral scouring. For conical obstacles placed in a wind tunnel, Okamoto *et al.* (1977) found a critical inclination of 15–30°, below which the horseshoe vortex completely ceases to persist. Bozkus and Yildiz (2004) conducted an experimental study on local inclined model bridge piers but only investigated inclinations between 75 and 88°. They show that non-dimensional scour depth (scour depth relative to pier diameter) decreases linearly under a given Froude number ($Fr = U_m(d_w g)^{-1/2}$, with U_m = mean flow velocity, d_w = water depth and g = gravitational acceleration) with increasing pier inclination. Quantitative studies on sedimentary structures at strongly inclined cylinders embedded in a sedimentary layer, while being exposed to water flow, are still lacking, however.

Permeability

Plant permeability, arising from multiple or bifurcated stems, may probably not be a direct adaptation to flood stresses, but systematic fluid mechanical lab studies suggest that an increasing permeability leads to an increased amount of bleed flow (i.e. flow penetrating the obstacle), weakening of the horseshoe vortex and increasing length of the recirculation zone in the obstacle wake (Castro, 1970; Dong *et al.*, 2008; Leu *et al.*, 2008). The latter denotes a leeside region, where those currents that have detached from the obstacle exhibit a reversal flow behaviour, because of low pressures in the central near wake. All this favours net-deposition of fine sediments and reduces frontal scouring (Allen, 1984; Leenders *et al.*, 2007; Figure 1a). Examples of obstacle marks forming at shrubs have been reported by Nakayama *et al.* (2002). The permeability of a plant depends on several factors: first, the number and size of stems and leaves per unit area, controlled by age and growth season, play an important role. For example, shrub permeability increases by defoliation. Second, if the

stems are flexible the projected frontal area decreases in size under flood exposure (e.g. Rodrigues *et al*., 2007; Schnauder & Moggridge, 2009). At the same time, the permeability decreases as well because stems and leaves are compressed. Third, the permeable part of the plant body reduces in permeability, when sediments or debris transported as bed-, suspended- or floating-load get entangled between the stems and leaves, generating an armouring effect (Nakayama *et al*., 2002). Measuring the permeability of a plant's cross-sectional projected frontal area may prove difficult under field conditions as the spatial arrangement of stems is usually complicated. However, one possible way is to measure the volumetric porosity, being the ratio between porous space and body volume (e.g. Grant & Nickling, 1998). The disadvantage here is that plants have to be completely removed to achieve this. A second method is to determine the 'optical' porosity of the projected frontal area of the plant, which is the open area divided by the total area (e.g. Grant & Nickling, 1998), for example, by employing digital photography.

The transfer of the above-mentioned fluid mechanical lab studies on flow processes around permeable obstacles in riverbeds is problematic because these experimental studies were conducted under flat bed conditions, that is, without sediments: moving sediments change the surface topography, which in turn significantly influences the hydraulic processes. In case of fluvial obstacle marks, this specifically applies to the magnitude and spatial extension of horseshoe and wake vortices, which are considerably affected when a frontal scour hole is present (Kirkil & Constantinescu, 2010; Euler, 2012).

Working hypotheses

The above outlined considerations lead to the main working hypotheses of this work:

a) With increasing inclination in streamwise direction and increasing permeability of the plant body, frontal scouring decreases and local scouring shifts laterally into the downstream direction, while the deposition of sediments at the leeside of the plant is promoted.
b) The amount of deposited sediments at the leeside can be analytically determined, when incorporating the most influential independent variables, including inclination and permeability. These variables can be deduced from empirical process studies.
c) Biomechanical adaptations to flood stresses and sediment flow enable woody riparian plants to control the initiation of pioneer island formation and favor the creation of new micro-habitats.

To test these hypotheses, a combined lab and field study was herein carried out. First, two experimental series were conducted in a laboratory flume to investigate the effect of inclination and permeability on sedimentary structures around models of plants. Such flume studies offer the advantage that both hydraulic and sedimentary processes and their dynamical interaction can be systematically investigated under controlled boundary conditions. Second, morphologies of obstacle marks that have developed at adult black poplars (*Populus nigra*) and willows (*Salix* spp.*)* in ephemeral secondary channels of the Loire River near Tours (France) were surveyed for comparison and up-scaling of lab measurements.

EXPERIMENTAL STUDY

Experimental design and boundary conditions

The two series of experiments were conducted in a 5.0×0.32 m (L × W) laboratory flume. The first series aimed at the effects of obstacle inclination and the second of obstacle permeability on processes of local scour and deposition around solitary riparian plants. A more detailed description of the flume is provided in Euler and Herget (2011). For each experimental run (in both series), one obstacle was centrally mounted on the flume bottom, 2.7 m downstream from inlet and embedded into an 8-cm thick layer of uniform coarse sand with a D_{50} (=median particle diameter) of 0.75 mm and a geometric standard deviation of the particle size distribution ($\sigma_g = (D_{84}/D_{16})^{1/2}$) of 1.3. The initial bed was flattened and compacted, and the obstacles were then exposed to steady, uniform flow for 24 h (series 1) and 28 h (series 2) to attain near steady state conditions of the developing sedimentary structures. During all runs, clear water conditions prevailed. This ensured an undisturbed view on the effect of obstacle characteristics only. A non-contact discharge meter allowed measurement of mean flow velocities, whereas a '*Vectrino*' ADV (acoustic Doppler velocimeter) by *Nortek* provided point data of three-dimensional flow velocities arising around the obstacles. The same instrument was also used to determine the undisturbed mean bed shear stresses, applying the turbulent kinetic energy approach (Biron *et al*., 2004). In addition, a flow tracer, introduced by Hoyt and Sellin (2001), was applied for qualitative flow visualization around the cylinders. After the end of each experiment, the flume was carefully drained, and the final bed topography was surveyed with a laser distance sensor by *Baumer* (accuracy: 0.1 mm) to create three-dimensional surface models of the bedforms (cf. Euler and Herget, 2012).

For the first series, three types of emergent aluminium cylinders with diameters of 0.01, 0.015 and 0.02 m and a uniform length of 0.35 m were screwed to a plate at the flume bottom that allowed adjustment of the inclination and safe removal of the cylinders without disturbing the final bedform. Inclinations of 20°, 25°, 30°, 45° and 60° were chosen, giving a total of 15 runs (Table I). In all 15 runs, a flow velocity of 0.28 ms^{-1} and a water depth of 0.08 m was set.

In the second series, three types of cylindrical obstacles with equal dimensions (height above initial plane bed: 0.015 m, diameter: 0.03 m) but different permeabilities were used: although one group of cylinders was

Table I. Experimental boundary conditions and results. w_o = obstacle width, α = inclination in streamwise direction, d_w = water depth, T = water temperature, U_m = mean flow velocity, U_t = tip-velocity, τ_0 = bed shear stress, d_{s_max} = maximum scour depth, x dist = position of maximum scour depth in streamwise direction and relative to cylinder centre, w_s = width of scour hole, l_s = length of scour hole, l_r = length of ridge, h_r = height of ridge, w_r = width of ridge, Vol. (-) = eroded sediment volume, Vol. (+) = deposited sediment volume. C = cylinder, PB = plain brush, BSW = brush with steel-wool

(unit)		m	°	m	°C	ms^{-1}	ms^{-1}	Nm^{-2}	m	m	m	m	m	m	m	m^3	m^3
no	type	w_o	α	d_w	T	U_m	U_t	τ_0	d_{s_max}	x dist	w_s	l_s	l_r	h_r	w_r	Vol. (-)	Vol. (+)
1	C	0.010	20	0.08	22	0.28	0.28	0.196	0.010	0.005	0.045	0.070	0.055	0.001	0.025	0.000033	0.000033
2	C	0.010	25	0.08	21	0.28	0.28	0.196	0.011	0.022	0.083	0.083	0.120	0.005	0.073	0.000031	0.000027
3	C	0.010	30	0.08	22	0.28	0.28	0.196	0.011	0.000	0.058	0.073	0.060	0.004	0.038	0.000016	0.000014
4	C	0.010	45	0.08	22	0.28	0.28	0.196	0.016	-0.010	0.103	0.115	0.125	0.005	0.060	0.000082	0.000038
5	C	0.010	60	0.08	21	0.28	0.28	0.196	0.018	-0.020	0.130	0.167	0.195	0.010	0.088	0.000140	0.000079
6	C	0.015	20	0.08	22	0.28	0.28	0.196	0.018	0.005	0.070	0.090	0.126	0.003	0.055	0.000007	0.000003
7	C	0.015	25	0.08	21	0.28	0.28	0.196	0.007	0.005	0.045	0.060	0.040	0.006	0.058	0.000007	0.000005
8	C	0.015	30	0.08	21	0.28	0.28	0.196	0.014	-0.003	0.135	0.120	0.100	0.010	0.140	0.000084	0.000074
9	C	0.015	45	0.08	22	0.28	0.28	0.196	0.026	-0.011	0.135	0.130	0.280	0.007	0.110	0.000145	0.000115
10	C	0.015	60	0.08	21	0.28	0.28	0.196	0.024	-0.025	0.175	0.190	0.360	0.010	0.165	0.000255	0.000213
11	C	0.020	20	0.08	21	0.28	0.28	0.196	0.012	0.050	0.110	0.095	0.260	0.006	0.116	0.000068	0.000060
12	C	0.020	25	0.08	21	0.28	0.28	0.196	0.019	0.013	0.113	0.133	0.170	0.011	0.100	0.000089	0.000077
13	C	0.020	30	0.08	21	0.28	0.28	0.196	0.019	-0.004	0.125	0.128	0.210	0.010	0.110	0.000094	0.000086
14	C	0.020	45	0.08	22	0.28	0.28	0.196	0.028	-0.023	0.174	0.185	0.320	0.007	0.175	0.000247	0.000210
15	C	0.020	60	0.08	21	0.28	0.28	0.196	0.034	-0.040	0.200	0.220	0.460	0.009	0.200	0.000378	0.000319
16	PB	0.030	90	0.11	20	0.28	0.26	0.163	0.030		0.139	0.048	0.426	0.009	0.182	0.000288	0.000288
17	BSW	0.030	90	0.11	16	0.28	0.26	0.163	0.039		0.170	0.059	0.490	0.010	0.220	0.000439	0.000439
18	C	0.030	90	0.11	19	0.28	0.26	0.163	0.040		0.182	0.065	0.575	0.010	0.245	0.000520	0.000520
19	C	0.030	90	0.11	18	0.25	0.22	0.120	0.028		0.124	0.048	0.180	0.014	0.167	0.000134	0.000134
20	BSW	0.030	90	0.11	19	0.25	0.22	0.120	0.021		0.094	0.035	0.148	0.008	0.119	0.000059	0.000059
21	PB	0.030	90	0.11	21	0.25	0.22	0.120	0.022		0.097	0.035	0.137	0.010	0.130	0.000065	0.000065
22	PB	0.030	90	0.11	20	0.22	0.18	0.095	0.007		NV	NV	0.000	0.000	0.030	0.000009	0.000009
23	BSW	0.030	90	0.11	21	0.22	0.18	0.095	0.007		NV	NV	0.070	0.005	0.030	0.000009	0.000009
24	C	0.030	90	0.11	19	0.22	0.18	0.095	0.020		0.088	0.032	0.085	0.011	0.125	0.000045	0.000045
25	C	0.030	90	0.08	18	0.25	0.23	0.100	0.028		0.121	0.046	0.180	0.010	0.166	0.000124	0.000124
26	BSW	0.030	90	0.08	18	0.25	0.23	0.100	0.026		0.113	0.043	0.170	0.010	0.143	0.000097	0.000097
27	PB	0.030	90	0.08	18	0.25	0.23	0.100	0.023		0.103	0.036	0.145	0.012	0.143	0.000091	0.000091
28	PB	0.030	90	0.08	19	0.22	0.21	0.116	0.010		0.059	0.015	0.056	0.004	0.072	0.000011	0.000011
29	BSW	0.030	90	0.08	19	0.22	0.21	0.116	0.004		0.044	0.010	0.073	0.003	0.028	0.000007	0.000007
30	C	0.030	90	0.08	18	0.22	0.21	0.116	0.026		0.113	0.043	0.131	0.012	0.144	0.000090	0.000090

impermeable and made of brass, the other two obstacles were industrial brushes with brass bristles (Figure 2). The only difference between these latter two was that into one of the brushes, steel wool was additionally embedded to decrease the permeability. Permeabilities were determined using the volumetric and the optical porosity measurement approach. To measure the volumetric porosity, the brushes were submerged into a measuring glass and compared with the volume of the brass cylinder. The optical porosity was defined following the method applied by Grant and Nickling (1998). Hence, digital photographs of both brushes were taken in front of a black background. Next, the contrast of each picture was enhanced so that only black and white pixels remained. For better results, the brightness of the picture was also increased. Finally, a representative part of the picture was cut out, and via a histogram, the percentage of black and white pixels could be determined (Figure 2). These procedures revealed that the plain brush (PB) had a volumetric porosity of 7% and an optical porosity of 25%, whereas the brush with steel wool (BSW) had a volumetric porosity of 9% and an optical porosity of 35%. Different flow boundary conditions were set for the experiments, consisting of five stages with flow velocities of 0.22, 0.25 and 0.28 ms^{-1} and water depths of 0.08 and 0.11 m (Table I). Because the obstacles were deeply submerged during all experiments of series two, the water surface remained undisturbed. Hence, it was possible to additionally survey the rate of scour depth incision using the laser distance sensor. The deflection of the punctual laser beam through a water column is linear and could be corrected using appropriate linear functions.

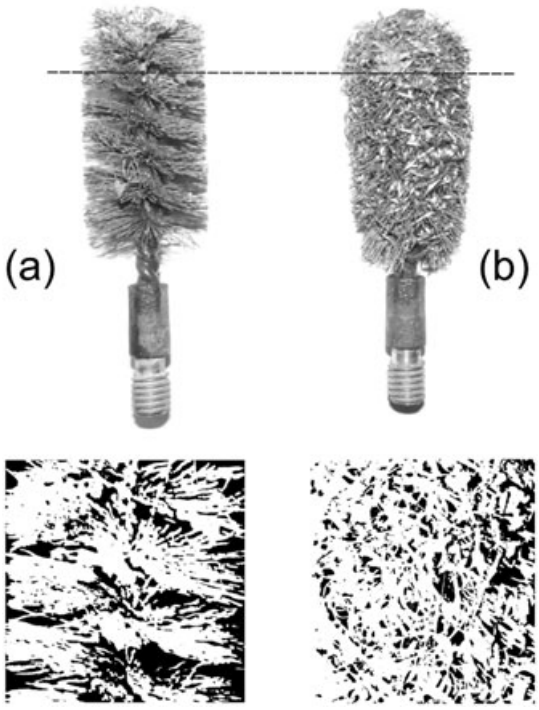

Figure 2. Brushes used as obstacles for the permeability experiments and optical porosities. (a) Plain brush (PB); (b) brush with steel-wool (BSW). Diameter of brushes is 0.03 m. The dotted line indicates the level of the initial plane bed

Field study

The floodplains of the anabranching Loire River near the city Tours in France contain several secondary channels that become inundated during flood events only (Rodrigues *et al.*, 2006). These channels are basically composed of coarse sandbeds and feature in-channel woody vegetation, mainly black poplars and willows. When exposed to flood flows, the trees induce the formation of obstacle marks, which persist even when the channels drain after flood recession (Rodrigues *et al.*, 2007). The last major flood event reached a maximum discharge of 1950 m^3s^{-1} (gauging station of Langeais located 4.5 km upstream), which corresponds to a 1-in-two year flood. This event caused inundation of the channels and occurred six months prior to the field investigations. Nine obstacle marks in three different secondary channels, named herein I, II and III, were selected for investigation. Length and widths of these channels are between 600 and 700 m and 60 and 90 m (Figure 3).

Rodrigues *et al.* (2006) already investigated the meso-scale sedimentary and hydraulic process dynamics during flood flows in channel I in detail. Since 2000, this channel was flooded 18% of time, mostly in winter. During the highest discharge, mean flow velocities in the channel ranged from about 0.7 to 1.0 ms^{-1} (Rodrigues *et al.*, 2006). Because of a low critical threshold of motion, the according bed shear stresses induce bedload transport, even at low discharges. For the present study, five obstacle marks in channel I and two obstacle marks each in channels II and III were surveyed. Because of reasons of simplicity, only solitary black poplar and willow trees were taken into consideration. None of the obstacle marks showed signs of post-flood disturbances, e.g. by animal activity. Because the field work was conducted in June (2011), all trees had fully developed leaves. The detailed morphologies of the bedforms around the trees were recorded with a *Zeiss Elta C30* total station. These data were then used to create digital elevation models of the obstacle marks, using the software *Surfer 8* by *Golden Software*, so that calculation of scoured and deposited volumes of sediments could be performed. For spatial interpolation, 'radial basis function' was chosen.

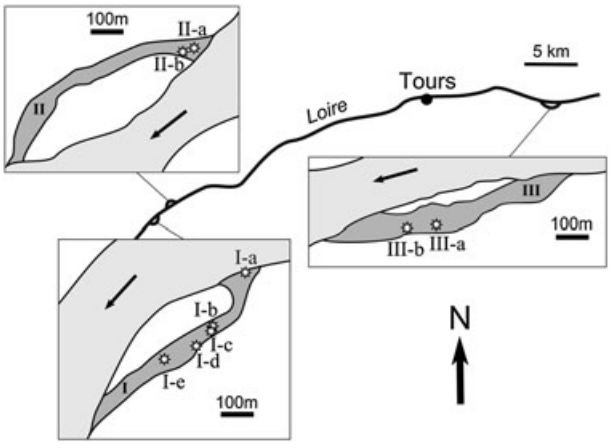

Figure 3. Secondary channels I–III of the Loire River near the city of Tours (France). The stars mark the locations of the surveyed obstacle marks

In addition, the size and inclination of the projected frontal area of each tree was recorded manually and supplemented by digital photographs. Inclinations (in streamwise direction) were measured with a digital slope level. Photographs were also taken to approximate the optical porosity of the trees. Scour depths as well as sediment ridge lengths, height and widths were additionally measured by tape. To assess the spatial variabilities of sediment grain size distributions, bulk sediment samples were each taken at three locations: First, 1–2 m upstream of the plant, second, at the mid-central part of the leeside sediment accumulation and third, in the horseshoe vortex and scour hole region laterally of the trees. The samples were later processed by standard sieving analysis.

Flood deposits, such as woody debris caught between the stems, served as high-water marks so that maximum local water depths could be determined. However, only those deposits were considered that were found in inflexible parts of the trees to exclude misinterpretation. For estimation of hydraulic boundary conditions during formation, existing topographic surveys were used for one-dimensional flow simulation of peak discharges using *HEC-RAS 4.1* (*Hydrological Engineering Center*, *US Army Corps of Engineers*; Brunner, 2002). The known flow depths were used as input boundary conditions. Limitations and uncertainties of this method are discussed in Carling *et al*. (2003). Because such topographical data were not available for channel III, channel cross sections in front of the trees and the local bed slopes were measured using the total station. In combination with the water depth values, this enabled estimation of approximate mean flow velocities by application of the Manning equation. Roughness values (i.e. n values) were chosen in reference to those values applied by Rodrigues *et al*. (2006).

RESULTS

Inclination

Determination of mean bed shear stresses with the ADV instrument revealed that the flow conditions during experiments 1–15 were close to the initiation of grain movement, with $U_m U_c^{-1} = 0.98$ (with U_m = mean flow velocity; U_c = critical flow velocity for initiation of sediment transport, corresponding a bed shear stress of $0.20\,Nm^{-2}$). In all runs, sediment displacements occurred around the cylinders. The morphometries of the resulting bedforms are specified in Table I. Their spatial patterns, however, varied significantly and revealed a strong influence of cylinder inclination, as the digital surface models in Figure 4 display. Compared with the scour patterns around straight bridge piers, the frontal scour hole increasingly shifted into the downstream direction with increasing cylinder inclination, up to a point where scouring took place in the wake region of the obstacle only. Maximum scour depth locations were then no longer found centrally in front of the cylinder, but laterally, and on average shifted downstream by 0.6 cm per 5° inclination (Figure 5c). When inclinations of 20° prevailed, the total sediment movement (erosion and deposition) around the obstacles were reduced by 83%, compared with inclinations of 60° (in the mean ca. 8–10% per 5°). On average, maximum scouring linearly reduced by 0.2 cm and ridge lengths by 3.0 cm per 5° cylinder inclination. With decreasing inclinations, the relation between scoured and deposited volumes of sediments turned negative (Figure 5d).

The considerable change in sedimentary patterns matches a distinct change of flow patterns, with horseshoe vortex domination at low inclinations and wake vortex domination at strong inclinations. In cases of horseshoe vortex domination (Figure 5b), strong turbulent uplifting motions in the obstacle wake force some of the eroded particles into suspension, which explains the deficit of deposited compared with scoured volume here. Figure 5 (e) displays a comparison between z-velocities close to the projected frontal areas at different inclinations and equal cylinder diameters. From this illustration, it becomes evident that the amount of flow deflection at the cylinder front reduced with increasing cylinder inclination. Tracer observations supported these measurements. At inclinations between 25 and 30°, the horseshoe-vortex system ceased to persist completely (Figure5a).

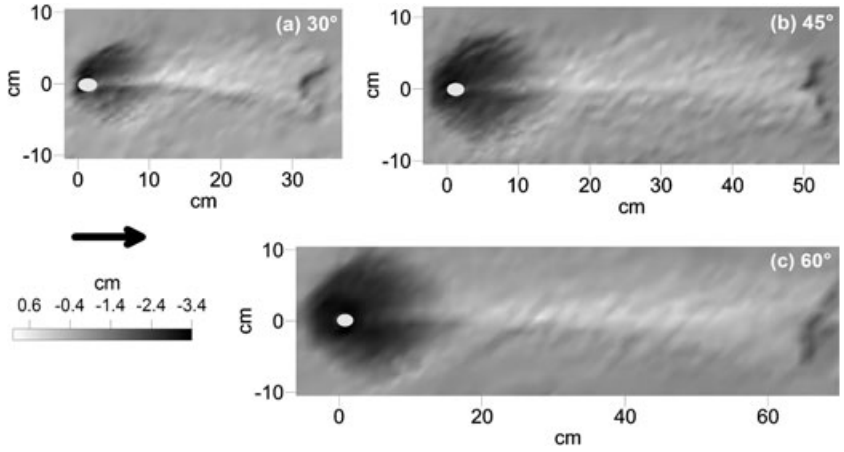

Figure 4. Influence of cylinder inclination on bed morphology under steady flow conditions (flow velocity and water depth = 0.28 ms^{-1} and 0.08 m, respectively). (a) High inclination, (c) low inclination

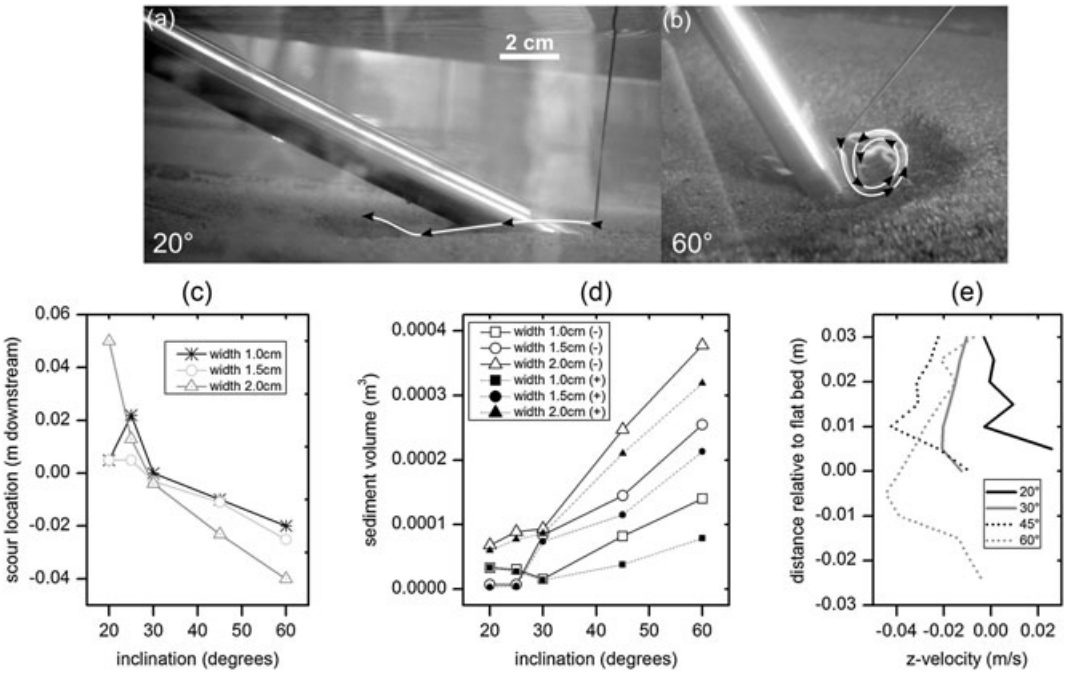

Figure 5. (a,b) Influence of cylinder inclination on the local flow field, visualized by tracer injections; (c) shift of maximum scour depth in streamwise direction relative to the cylinder centre; (d) eroded (-) and deposited (+) sediment volumes under different cylinder inclinations and diameters; (e) vertical distribution of z-velocities 0.05 m upstream of cylinder centre in dependence of inclination

These values hence mark a critical threshold between the two states. Instead, the currents were then laterally diverted when hitting the obstacle, detached behind the obstacle and formed leeside wake vortices that led to scouring in the wake region.

Although the amounts of deposited sediments leeside of the scoured zones considerably differed, the sediment ridges had similar shapes, independently from cylinder inclination (Figure 4). Furthermore, different cylinder diameters also affected the amount of eroded and deposited material. Hence, when wider cylinders were used, more sediment was eroded and deposited in comparison to smaller cylinders as Figure 5(d) additionally reveals.

Permeability

During the experiments, focussing on obstacle permeability (runs 16–30), shear stresses between 0.095 and 0.163 Nm^{-2} were measured, resulting in relations between $U_m U_c^{-1}$ from 0.475 to 0.815 so that clear-water conditions prevailed in all runs. Two states of obstacle marks developed in the course of this series: first, typical obstacle marks with frontal scouring and leeside sediment deposition (runs 16–21, 24–27, 30; Figure 6a,b) and second, leeside scouring with adjacent sediment deposition (runs 22, 23; Figure 6c).

In runs 28 and 29, a transition between both states was observed, featuring imperfectly developed frontal scour

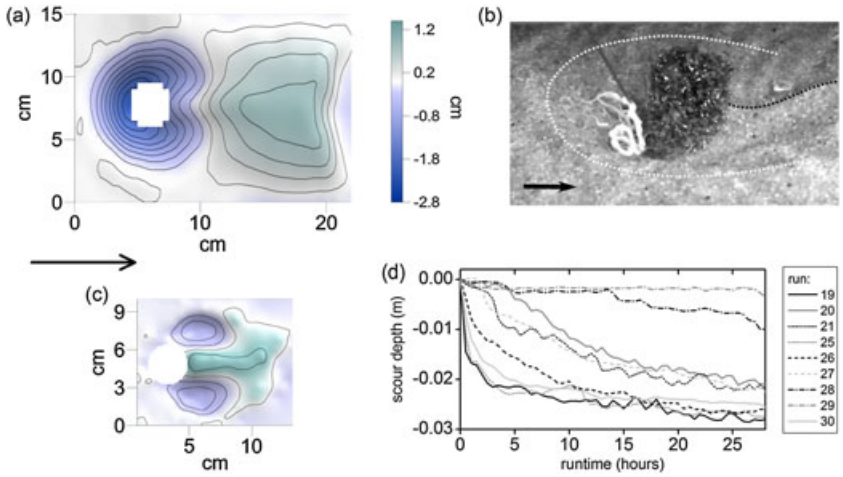

Figure 6. Morphological states in dependence of obstacle permeability and flow conditions. (a) Obstacle mark at the plain brush in run 21, with characteristic frontal scour hole and leeside sediment ridge (flow velocity = 0.25 ms^{-1} and water depth = 0.11 m); (b) visualization of downflow and horseshoe vortex by flow tracer injection in the scour hole in front of the brush with steel-wool (run 26); (c) lateral leeside scouring in run 23 at the brush with steel-wool (flow velocity = 0.22 ms^{-1} and water depth = 0.11 m); (c) trajectories of temporal frontal scour depth development during selected runs

holes as well as partial leeside scouring, hence marking a critical threshold condition. All marks that formed around the obstacles, however, had more or less balanced relationships between eroded and deposited volumes (cf. Table I). Those forms characterized by leeside scouring (second state) only developed with permeable obstacles and mean flow velocities of 0.22 ms^{-1}. In general, when water depth was decreased, while mean flow velocity was kept constant, 'tip-velocities' (i.e. those velocities directly approaching the submerged obstacle) slightly increased (cf. Table I), and simultaneously, the input of kinetic energy approached the obstacle. When full obstacle marks formed, a reductive influence of the permeable brushes compared with the solid cylinders became apparent. On average, the plain brush had a reducing effect of 59% and the brush with steel-wool of 69% on eroded and deposited volumes. The ranges of reduction, however, varied between 49 and 73% for the plain brush and between 44 and 84% for the brush with steel wool. A second observation was that the initiation of scour incision was delayed when permeable obstacles were used, which explains the range of variabilities stated above. In this context, Figure 6(d) depicts selected temporal trajectories of the (non-linear) scour incisions. Although obstacle marks that formed under the influence of brushes were smaller than those forming at the cylinder, the general bedform shape and hydraulic processes were identical. Hence, downflow, horseshoe vortex system and wake flow could be clearly identified from the hydraulic measurements, independently from obstacle type (Figure 6b, 7a). With permeable obstacles, bleed flow was then occurring at the upper lateral parts of the brushes only, as the majority of the approaching current was pushed downwards in front of the brushes. Furthermore, current recirculation in the obstacle wake was not existent, and thus, a change of recirculation length in dependence of obstacle permeability, as known from flat bed studies, could not be observed. Considering Figure 7(a,c), currents in the obstacle wake showed an upward direction, when obstacle marks formed. This matches previous observations (Euler, 2012).

In the second observed state, horseshoe vortex-related frontal scouring did not develop. Instead, the separated currents indeed recirculated in the wake zone of the obstacle, thereby causing the formation of two opposite scour pockets (cf. Figure 6c). Figure 7(b,c) reveals this leeside reversal of flow and clearly indicates the zone of current recirculation. Also, a higher amount of bleed flow moving through the brushes was visible under these conditions from tracer observations. The resulting bed morphologies in runs 22 and 23 generally showed little derivation from each other so that the effect of differing obstacle permeabilities was minimal here.

Field results

All relevant results of the field survey are listed in Table II, including morphometric, sedimentary and hydraulic data. Figures 8 and 9 depict pictures and surface models of selected obstacle marks in the three secondary channels, revealing characteristic biogeomorphic features of these bedforms.

Five of the nine investigated obstacle marks had a significantly positive relationship between deposited and eroded sediments. Concerning the remaining four obstacle marks, this relationship was balanced. The obstacle sizes specified in Table II each refer to the (approximate) frontal area that was exposed to flow during the last flood event. In most cases, the projected frontal areas of the trees consisted of inflexible woody stems, containing flood-related woody debris (Figure 10a) and sparse leaf growth. These jams increased the obstacle width and decreased the permeability. Determination of the optical porosities resulted in values between 7 and 20% (mean: 13%, see Table II and Figure 10a). All poplar trees that were considered featured stable, inflexible trunks.

Channel I. The five obstacle marks surveyed in channel I (denoted I-a to -e) had formed around adult black poplar trees. Flow simulations indicated mean flow velocities between 0.75 and 0.8 ms^{-1} during the last flood in the channel (discharge = 100m^3s^{-1} in the secondary channel). The obstacle marks each featured streamlined

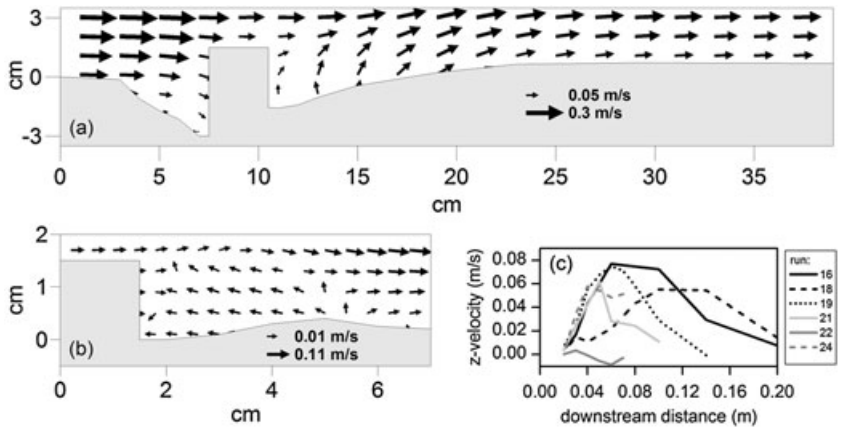

Figure 7. Differences of 2D flow velocities along the plane of symmetry in dependence of prevailing system state: (a) run 16 – frontal scouring, downflow, horseshoe vortex and turbulent uplifting fluid motions in the wake; (b) run 22 – leeside scouring and flow reversal in the wake. Obstacle in each case is the plain brush; (c) leeside longitudinal distribution of z-velocities at the plane of symmetry, 0.015 m above the plane bed (selected runs only)

Table II. Field results. por. = porosity, h_o = obstacle height. D_{50} denotes median sediment size upstream of the trees; σ_g is the geometric standard deviation of the grain size distribution. Locations of sediment sampling: A = upstream of plant, B = sediment ridge, C = region of horseshoe-vortex. All other abbreviations are identical with those in Table I

(units)	m/s	m	m		°		%	m		m	m	m	m	m		m	m^3	m^3
name	U_m	h_o	w_o		α		por.	d_s		l_s	w_s	l_r	w_r	h_r			vol +	vol -
			min	max	min	max		front	max					min	max			
I-a	1.3	2.5	3.3	4	75	80	15.5	NV	NV	NV	NV	28	3.8	0.4	0.6		30	NV
I-b	0.75	1.7	0.8	0.8	80	90	15	NV	NV	NV	NV	13.1	3.1	0.25	0.25		5	0.8
I-c	0.75	2.1	1.4	1.4	75	85	11.5	0.3	0.3	0.6	3.5	9.8	4.2	0.3	0.5		4.8	3.9
I-d	0.8	1.9	0.4	0.5	65	90	20	0.25	0.3	0.6	1.8	6.2	1.6	0.15	0.15		0.4	0.3
I-e	0.8	1.3	0.7	0.7	25	90	11.5	NV	NV	NV	NV	11.5	2.5	0.25	0.4		1.5	0.3
II-a	0.65	2.7	1.6	1.6	50	90	14	NV	NV	NV	NV	13	3.9	0.9	1		13.3	0.3
II-b	0.75	2.5	1.2	1.2	55	80	7	0.3	0.6	0.8	4	16	5	0.35	0.4		6.5	6
III-a	1.1	1.6	1.7	1.7	75	90	9	0.1	0.3	0.4	2	27.5	6.2	0.2	0.3		41	15
III-b	1.25	0.5	1.7	1.7	40	50	12	0.25	0.25	0.9	2.5	7.8	4	0.4	0.5		5.6	0.3

(units)	mm	mm	mm			
name	D_{50_A}	D_{50_B}	D_{50_C}	σ_{g_A}	σ_{g_B}	σ_{g_C}
I-a	15	1.1	300*	4.7	1.5	NV
I-b	1.1	0.9	1.7	1.7	2.1	4.2
I-c	1.7	1.1	3.5	2.1	2.5	4
I-d	1.3	1.3	3.4	2.6	2.3	3.4
I-e	1.4	2	NV	3.2	2.9	NV
II-a	13.5	0.3	NV	5.8	1.6	NV
II-b	3.5	9	15.5	7.3	4.9	3.7
III-a	1.2	1	3.1	2.8	2.5	7.4
III-b	1.6	0.9	2.3	2.4	1.9	2.3

*rip rap.

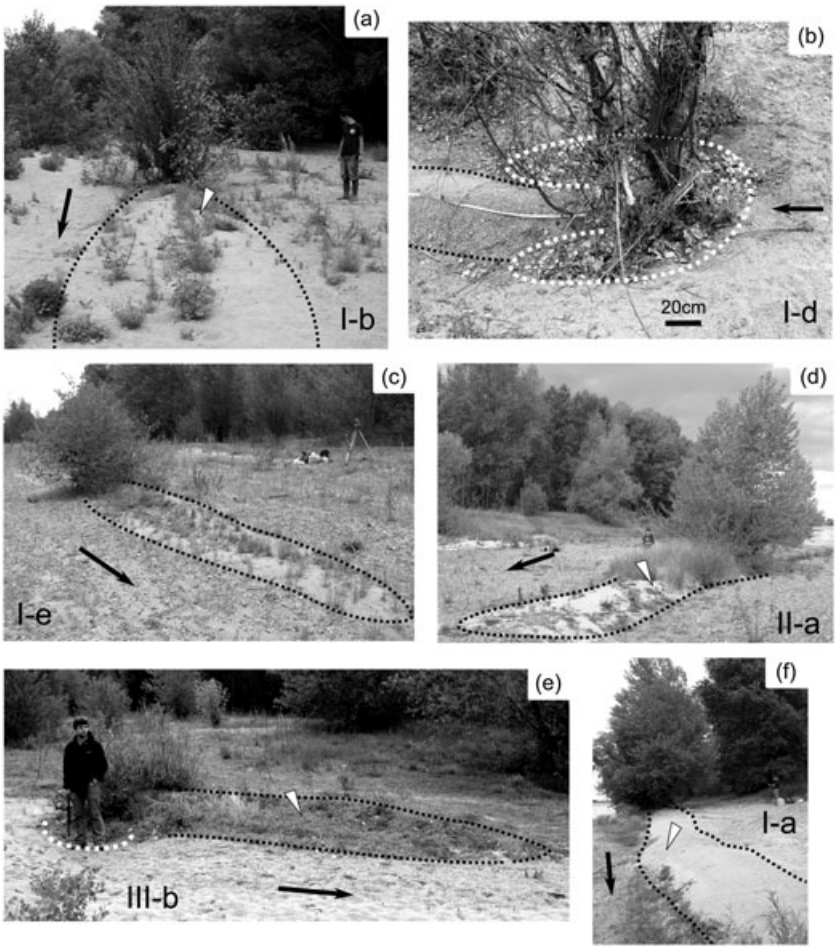

Figure 8. Selected obstacle marks at poplar (a–d, f) and willow (e) trees in the three secondary channels of the Loire river showing typical erosional and depositional features and growth of pioneer vegetation on top of the sediment ridges (only a, c, d and e). The roman numbers refer to the reach number and the letters to the obstacle mark number (cf. Table II). Arrows indicate flow directions. Note persons and tripod for scale [Species growing on the ridges and date of colonization: obstacle mark Ib – annual plants (*Xanthium orientale*, *Plantago arenaria*, colonization during 2011); obstacle mark Ie – *Oenothera* (at least since 2010); obstacle mark IIa – *Carex spp*. (date of colonization unknown); IIIb – grasses and annual plants (growing for at least 2 or 3 years before 2011).]

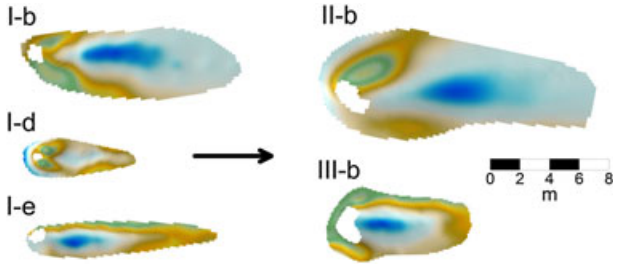

Figure 9. Surface models of selected surveyed obstacle marks in secondary channels of the Loire River (France). The roman numbers refer to the reach number and the letters to the obstacle mark number (cf. Table II)

depositional sediment ridges, whereas I-c, I-d and I-e also included local scour holes. Here, maximum scour depths were predominantly located laterally of the trees (Figure 8b, 9). Stem inclinations ranged from 25 to 90°, whereas merely the lower, basal parts (up to about 0.5 to 1 m above the ground) were strongly inclined (Figure , 8b, 10b). Because obstacle mark I-a was located at a low elevation close to the main channel of the Loire river in the entrance region of the secondary channel, a regular flood exposure is almost certain (Figure 8f). No other vegetation was growing on the ridge here, and the ridge was composed of nearly uniform coarse sand (Figure 10c). Rip-rap remnants upstream of the poplar with mean diameters of 300 mm prevented frontal scouring. At this location, the mean flow velocity was directly measured during the last flood (1.3 ms^{-1}). However, the other four obstacle marks were all located inside the secondary channel, and their ridges were to some extent colonized by grass and juvenile vegetation, mostly following a longitudinal strip along the central ridge (Figure 8a,c). Outcrops revealed complex cross stratified structures made of fine gravel to coarse sands and sometimes topped by layers of mud within the ridges of I-b to I-e (Figure 10d). These muddy layers are related to receding flood flows and have already been described in detail by Rodrigues *et al*. (2007). Root networks ranging through the ridge bodies stabilized the deposited sediments. A comparison of the absolute and relative sedimentary data in the obstacle mark regions shows that within channel I, grain sizes and grading of the coarse sands upstream of

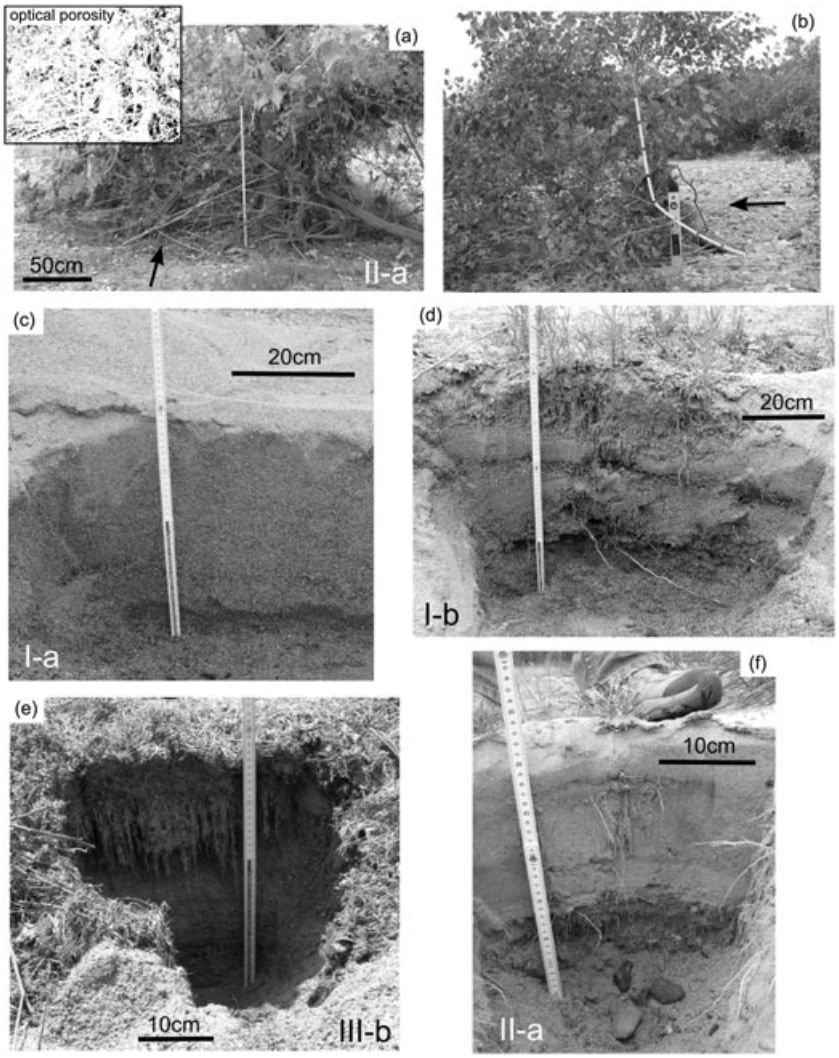

Figure 10. (a) Projected frontal area of a poplar tree with jam of woody debris and according optical porosity. (b) Inclination of the stem base of a young poplar growing in a secondary channel. Length of water level is 0.4 m. (c-f) Outcrops of selected sediment ridges, revealing the individual composition of the ridge bodies and the stabilizing function of a vegetation cover. The displayed roman numbers refer to the reach number and the letters to the obstacle mark number (cf. Table II)

the obstacles were similar to those sampled at the sediment ridges. In contrast, the sediments in the horseshoe vortex region were significantly coarser and poorly sorted.

Channel II. Obstacle marks II-a and II-b (Figure 8d, 9) both developed around adult black poplar trees. They were located directly within channel II but not far from the entrance region. Flow simulations resulted in mean flow velocities around 0.65 and 0.75 ms^{-1} in this part of the channel. In case of II-a, scouring was completely absent. Instead, a depositional ridge with a length of 13 m and a height of 0.9 m was present. Again, the projected frontal area of the poplar was jammed with woody debris. The main stem was inclined by 50° up to a height of 0.4 m. Above that, the plant grew nearly vertically. For the most part, the ridge was colonized with sedges (*Carex* spp.), which apparently increased the resistance against erosion and stabilized the ridge (Figure , 8d, 10f). The presence of the sedges led to trapping of fine and medium, nearly uniform sands on the ridge (Figure 10f). As a consequence, the D_{50} of the ridge material was by over 90% finer than the D_{50} of the surrounding gravelly sediments and much better sorted. Obstacle mark II-b featured significant scouring (max. -0.6 m), leading to a balanced relationship between local scouring and deposition (Figure 9, Table II). The main trunk had an inclination between 55 and 80°. All of the sediment sampled in the obstacle mark region consisted of gravel, whereas the ridge material (medium gravel) was around two times coarser but better sorted than the upstream material (fine gravel). The sediments within the scour hole were about four times coarser than those upstream of the scour hole.

Channel III. In the third channel, one obstacle mark (III-a) had formed around a large poplar, whereas the other one (III-b) had developed around a willow. Both were located in the thalweg of the channel. The flow computations resulted in mean flow velocities between 1.1 and 1.25 ms^{-1} here. Minor frontal scouring was recognizable in both cases, but the amount of leeside

accumulated sediment clearly predominated in each case (Table II). The basal part of the main trunk of III-a had an inclination of 75° up to a height of about 0.75 m. The sediments sampled from the ridge of III-a were not much different in size compared with those sampled upstream of the frontal scour hole (coarse sand), but layers of fine gravel were found within the ridge body by outcropping. On top of the ridge, a dried layer of mud was present, and patches of grass were growing there. Obstacle mark III-b was different from all other surveyed bedforms, as the 3- to 4-m wide basal part of the willow was densely armoured up to a height of 0.4 m with loam. The lower part of the plant was thus nearly impermeable, in contrast to the multiple, flexible stems above (Figure 8e). The projected frontal area of the basal part had an inclination of 40 to 50°. Because of a dense vegetation cover, mainly consisting of grass and moss, the streamlined sediment ridge with a height of 0.5 m was perfectly protected against erosion (Figure 8e). Furthermore, a muddy layer was topping the ridge. Outcrops showed that below the dense plant roots, the underlying coarse sands would be extremely prone to erosion without this organic protective layer as Figure 10e clearly illustrates. Grain sizes in the ridge region of III-b were two to three times finer than upstream of the obstacle.

Data integration

To find an integrative measure for estimation of the leeside sediment accumulation, several morphometric variables (ridge length, -height and -width) were correlated with deposited volume of sediment. The most significant (linear) correlation was achieved by using 'maximum ridge width' ($R^2 = 0.92$), independently from spatial scale and boundary conditions (Figure 11a). The maximum width of the sediment ridge offers the advantage that it is easy to measure in the field and additionally contains a high preservation potential. In contrast, for example, the variable 'maximum ridge length' was sometimes difficult to determine in the field because of downstream merging with sheets of bedload sediments.

For the analytical determination of the deposited sediment volume, a previously developed model (Euler and Herget, 2011) can be applied. Thereby, the projected frontal area is expressed as a length value (L_A), with $L_A = h_o^{2/3}\, w_o^{1/3}$, where h_o = obstacle height and w_o = obstacle width. This variable is then integrated in obstacle Reynolds number, $Re_o = U_m\, L_A\, \nu^{-1}$, where ν = kinematic viscosity. For consideration of the sedimentary influence, empirical correction factors for the upstream sediment size (K_{D50}) and gradation (K_σ) are applied as follows: if $w_o/D_{50} < 50$, then $K_{D50} = 1/(1 + (-\ 0.05\ (w_o/D_{50}) + 2.5))$, or if $w_o/D_{50} > 50$, then $K_{D50} = 1/(1 + (0.0003\ (w_o/D_{50}) - 0.01))$. K_σ is $1/\sigma_g$. Finally, Froude number (Fr) is incorporated so that the following functional relationship is given:

$$Volume\ \ dep.^{1/3} = a\left(\mathrm{Re}_0\ \ L_A Fr\ \ K_{D50}^2\ \ K_\sigma\right) b \qquad (1)$$

To quantify the effect of inclination, a correction factor for obstacle height of inclined emergent cylinders is herein proposed (K_α). It is based on the amount of deposited volume in dependence of inclination, as surveyed in the first series of the experimental study. The effective obstacle height (h_{eff}) may then be calculated from: $h_{eff} = h_o - ((90-\alpha)\ 0.012 h_o)$, where α = inclination into streamwise direction. To quantify the effect of permeability, a correction factor for the size of the projected frontal area (K_P) is suggested that is proportional to the percentage of optical porosity: K_P = (100-porosity in %) / 100. A given porosity of 20% would thus lead to the following: $K_P\, L_A = 0.8\, L_A$. Figure 11b depicts the analytically modelled values from Equation (1), including the corrections for inclination and permeability, against the cube root of deposited volumes for the field case. Although the ridge volumes were partly influenced by the presence of a pioneer vegetation cover, the model basically reflects the trend of the field data. However, considerably more field data will be needed to compute significant correlations for practical application of the model.

INTERPRETATION AND DISCUSSION

This study has shown that mechanical properties of riparian woody plants, streamwise inclination and permeability, lead to a reduction of horseshoe vortex stresses acting at the projected frontal area and hence to a reduction of frontal scouring. Moreover, with increasing inclination and permeability, the total amount of locally mobilized sediments significantly decreases. When obstacles are increasingly inclined in streamwise direction, patterns of scouring change

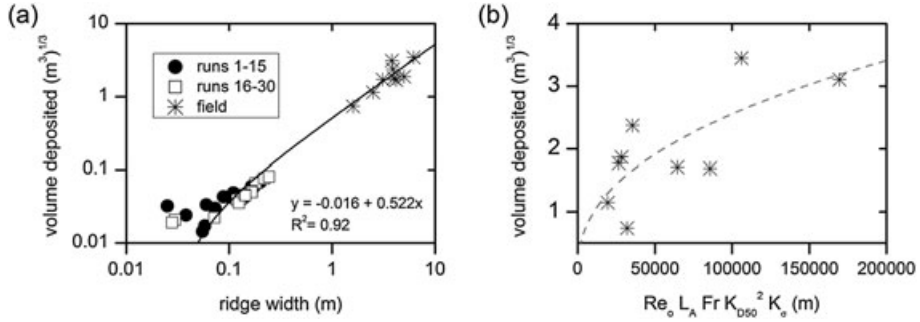

Figure 11. (a) Scale invariance and linear correlation of sediment ridge width against cube root of deposited sediment volume; (b) cube root of leeside deposited sediment volume *versus* analytical model values (Equation 1), including corrections accounting for obstacle inclination and porosity

and maximum scour depths shift downstream on both sides of the obstacle. At an inclination of around 25°, frontal scouring is reduced to an absolute minimum. Although permeable obstacle generally reduce frontal scouring, scour patterns are identical to impermeable obstacles when the threshold for frontal scouring is exceeded. By being inclined and partly permeable, riparian plants prevent local net erosion, while enabling downstream sediment deposition and, thus, the formation of new micro-habitats. Hence, the level of inclination and permeability plays an important role with respect to the ecosystem engineering function of riparian trees and the initiation of pioneer island establishment. The growth of pioneer vegetation on top of the ridges require phase without mechanical stresses arising from floods. However, if a vegetation cover (usually herbaceous plants) is present, the sediment bodies of the ridges consist of heterogeneous structures, including enclosures of fine sediments. The three initial working hypotheses were thus basically verified, although according plant-physiological processes of adaptation need further investigation from a biological point of view.

An explanation for the observed inclination of the basal parts of the polar trunks is that juvenile poplars easily bend under flood stresses but become more stable (i.e. woody) when they come of age (Figure 10b). Although the inclination at the base will persist, the adult trunk grows vertically in the direction of the sun then. What remains is a solidified lunate shape at the trunk base of the trees. In the field, similar spatial patterns of scouring were detected in comparison to the experiments, when trees featured inclination. Also, a consistency of sediment ridge widths across wide spatial scales became apparent (Figure 11a). These consistencies across spatial scales showed that the underlying hydraulic and sedimentary processes are similar and scale independent and may be related to self-organizing physical mechanisms. Physical self-organization is here defined as the dynamic interaction between hydraulic and sedimentary processes, leading to the emergence of macroscopic bedforms (see Euler, 2012). However, the field results furthermore showed that net deposition and preservation of sediments is considerably promoted, when the leeside sediment accumulation is colonized with a continuous cover of herbaceous vegetation. The establishment of a stabilizing vegetation cover in this zone requires periods without stresses arising from floods, ideally during the vegetative periods (cf. Gurnell *et al*., 2012). Apart from purely physical mechanisms, ecological aspects come into play here that create self-organized dynamics, controlled by specific patterns of plant succession and competition for resources (Francis *et al*., 2009). In future research on island development in rivers, it will thus be necessary to couple the physical self-organization of fluvial bedforms with the biological self-organization of riparian vegetation.

Eventually, the experimental results allowed adapting an existing analytical model for estimating the amount of deposited sediments leeside of solitary woody riparian plants in the field, assuming simplifying conditions. This analytical method is a first but novel attempt to model deposited sediments at the leeside of in-stream obstacles quantitatively. In this context, sediment ridge width proved to be a suitable estimator for leeside deposited sediment volume. This variable offers the advantage that it is robust with respect to post flood disturbances and sediment reworking, reaches steady state conditions very quickly and can be easily measured in the field. Although these finding are limited to small-scale phenomena, they may become important, if the abundance and assemblage of plant species in riparian areas is altered, for example, because of the spreading neophytes (e.g. Graf, 1978) or due to climatic changes.

It should be noted, however, that plant permeability and inclination as well as the width of the area exposed to flow can change throughout a flood event, mainly because of flood-related entanglements between the stems. Also, the permeability of a plant exposed to flood flows varies in dependence of growth season. In the present case, the flood that caused the formation of the investigated obstacle marks occurred in winter, whereas the field study was carried out in June. Hence, the obstacle permeabilities during the flood might have been slightly lower than estimated. Furthermore, it is hardly possible to determine, if post-flood obstacle marks in the field have reached true steady state conditions so that their morphometries can be related to those modelled in the flume. Direct measurements of obstacle mark dynamics in the field are not feasible. Nonetheless, near steady state conditions can be assumed in the present case, as local scouring primarily occurs during the rising limb of the hydrograph (Chang *et al*., 2004) and maximum scouring is reached rapidly, if mobile bed conditions prevail (Melville & Coleman, 2000). Both apply to the secondary channels of the Loire River near Tours. Anyway, a certain level of uncertainty will remain when applying the above-introduced analytical method and more comparative quantitative data from different types of rivers, and laboratory studies are needed for further validation.

ACKNOWLEDGEMENTS

The authors would like to thank Nicolas Claude, Coraline Wintenberger (both Université F. Rabelais de Tours) and Klaus Piesche (University of Bonn) for their technical support on the field and the 'Deutsche Forschungsgemeinschaft' (DFG) for project funding (project number: HE 3006/8-1). Moreover, the authors would like to thank two anonymous reviewers for their thorough and helpful comments on the manuscript. The manuscript of this article was part of the cumulative dissertation of Thomas Euler.

REFERENCES

Allen JRL. 1984. *Sedimentary structures*. Elsevier: Amsterdam.

Baker VR, Kochel RC. 1988. Flood sedimentation in bedrock fluvial systems. In *Flood Geomorphology*, Baker VR, Kochel RC, Patton PC (eds). Wiley: New York; 123–137.

Biron PM, Robson C, Lapointe MF, Gaskin SJ. 2004. Comparing different methods of bed shear stress estimates in simple and complex flow fields. *Earth Surface Processes and Landforms* **29**: 1403–1415.

Bozkus Z, Yildiz O. 2004. Effects of inclination of bridge piers on scouring depth. *Journal of Hydraulic Engineering* **130**: 827–832.

Brunner GW. 2002. *HEC-RAS, river analysis system hydraulic reference manual*. US Army Corps of Engineers: Davis.

Carling P, Kidson R, Cao Z, Herget J. 2003. Palaeohydraulics of extreme flood events: reality and myth. In *Palaeohydrology: Understanding Global Change*, Gregory KJ, Benito G (eds). Wiley: Chichester; 325–336.

Castro IP. 1970. Wake characteristics of two-dimensional perforated plates normal to an air-stream. *Journal of Fluid Mechanics* **46**: 599–609.

Chang WY, Lai JS, Yen CL. 2004. Evolution of scour depth at circular bridge piers. *Journal of Hydraulic Engineering* **130**: 905–913.

Corenblit D, Tabacchi E, Steiger J, Gurnell AM. 2007. Reciprocal interactions and adjustments between fluvial landforms and vegetation dynamics in river corridors: A review of complementary approaches. *Earth-Science Reviews* **84**: 56–86.

Corenblit D, Baas ACW, Bornette G, Delmotte S, Francis RA, Gurnell AM, Julien F, Naiman RJ, Steiger J. 2011. Feedbacks between geomorphology and biology controlling Earth surface processes and landforms: a review of foundation concepts and current understandings. *Earth-Science Reviews* **106**: 307–331.

Dong Z, Luo W, Qian G, Lu P. 2008. Wind tunnel simulation of three-dimensional airflow patterns around shrubs. *Journal of Geophysical Research* **113**: F02016.

Euler T, Herget J. 2011. Obstacle-Reynolds-number based analysis of local scour at submerged cylinders. *Journal of Hydraulic Research* **49**: 267–271.

Euler T, Herget J. 2012. Controls on local scour and deposition induced by obstacles in fluvial environments. *Catena* **91**: 35–46.

Euler T. 2012. Formation and dynamics of fluvial obstacle marks. Unpublished dissertation thesis, faculty of natural sciences: University of Bonn.

Fielding CR, Alexander J, Newman-Sutherland E. 1997. Preservation of in situ, arborescent vegetation and fluvial bar construction in the Burdekin River of north Queensland, Australia. *Palaeogeography, Palaeoclimatology, Palaeoecology* **135**: 123–144.

Francis RA. 2006. Allogenic and autogenic influences upon riparian vegetation dynamics. *Area* **38**: 453–464.

Francis RA, Corenblit D, Edwards PJ. 2009. Perspectives on biogeomorphology, ecosystem engineering and self-organisation in island-braided fluvial ecosystems. *Aquatic Sciences* **71**: 290–304.

Gibling MR, Davies NS. 2012. Palaeozoic landscapes shaped by plant evolution. *Nature Geoscience* **5**: 99–105.

Graf WL. 1978. Fluvial adjustments to the spread of tamarisk in the Colorado Plateau region. *Geological Society of America Bulletin* **89**: 1491–1501.

Grant PF, Nickling WG. 1998. Direct field measurement of wind drag on vegetation for application to windbreak design and modelling. *Land Degradation & Development* **9**: 57–66.

Gurnell A, Petts G. 2004. Trees as riparian engineers: The Tagliamento River, Italy. *Earth Surface Processes and Landforms* **31**: 1558–1574.

Gurnell A, Bertoldi W, Corenblit D. 2012. Changing river channels: The role of hydrological processes, plants and pioneer fluvial landforms in humid temperate, mixed load, gravel bed rivers. *Earth-Science Reviews* **111**: 129–141.

Hoyt JW, Sellin RHJ. 2001. Three-dimensional flow visualisation of large structures in the turbulent boundary layer. *Experiments in Fluids* **30**: 295–301.

Hupp CR, Osterkamp WR. 1996. Riparian vegetation and fluvial geomorphic processes. *Geomorphology* **14**: 277–295.

Karcz I. 1968. Fluvatile obstacle marks from the wadis of the Negev. *Journal of Sedimentary Petrology* **38**: 1000–1012.

Karrenberg S, Edwards PJ, Kollmann J. 2002. The life history of Salicaceae living in the active zone of floodplains. *Freshwater Biology* **47**: 733–748.

Kirkil G, Constantinescu G. 2010. Flow and turbulence structure around an in-stream rectangular cylinder with scour hole. *Water Resources Research* **46**: W11549.

Leenders JK, Boxel JH, Sterk G. 2007. The effect of single vegetation elements on wind speed and sediment transport in the sahelian zone of burkina faso. *Earth Surface Processes and Landforms* **32**: 1452–1474.

Leu JM, Chan HC, Chu MS. 2008. Comparison of turbulent flow over solid and porous structures mounted on the bottom of a rectangular channel. *Flow Measurement and Instrumentation* **19**: 331–337.

Melville BW, Coleman SE. 2000. *Bridge scour*. Water Resources Publications: Highlands Ranch.

Nakayama K, Fielding CR, Alexander J. 2002. Variations in character and preservation potential of vegetation-induced obstacle marks in the variable discharge Burdekin River of north Queensland, Australia. *Sedimentary Geology* **149**: 199–218.

Nanson GC, Knighton AD. 1996. Anabranching rivers: Their cause, character, and classification. *Earth Surface Processes and Landforms* **21**: 217–39.

Okamoto T, Yagita M, Kataoka S. 1977. Flow past cone placed on flat plate. *Bulletin of the Japan Society of Mechanical Engineers* **20**: 329–336.

Osterkamp WR, Costa JE. 1987. Changes accompanying an extraordinary flood on a sand-bed stream. In *Catastrophic Flooding*, Mayer L, Nash D (eds). Allen and Unwin: Boston; 201–224.

Osterkamp WR. 1998. Processes of fluvial island formation, with the examples from Plum Creek, Colorado and Snake River, Idaho. *Wetlands* **18**: 530–545.

Paola C. 2011. Co-evolution of rivers and plants. *Nature Geoscience* **4**: 583–584.

Rodrigues S, Bréhéret J-G, Macaire J-J, Moatar F, Nistoran D, Jugé P. 2006. Flow and sediment dynamics in the vegetated secondary channels of an anabranching river: The Loire River (France). *Sedimentary Geology* **186**: 89–109.

Rodrigues S, Bréhéret J-G, Macaire J-J, Greulich S, Villar M. 2007. In-channel woody vegetation controls on sedimentary processes and the sedimentary record within alluvial environments: a modern example of an anabranch of the River Loire, France. *Sedimentology* **54**: 223–242.

Rominger JT, Lightbody AF, Nepf HM. 2010. Effects of added vegetation on sand bar stability and stream hydrodynamics. *Journal of Hydraulic Engineering* **136**: 994–1002.

Schnauder I, Moggridge HL. 2009. Vegetation and hydro-morphological interactions at the individual plant, patch and channel scale. *Aquatic Sciences* **71**: 318–330.

Tal M, Paola C. 2010. Effects of vegetation on channel morphodynamics: results and insights from laboratory experiments. *Earth Surface Processes and Landforms* **35**: 1014–1028.

Tanaka N, Yagisawa J. 2010. Flow structure and sedimentation characteristics around clump-type vegetation. *Journal of Hydro-environment Research* **4**: 15–25.

Tooth S, Nanson GC. 2000. The role of vegetation in the formation of anabranching channels in an ephemeral river, Northern plains, arid central Australia. *Hydrological Processes* **14**: 3099–3117.

Unger J, Hager WH. 2007. Down-flow and horseshoe vortex characteristics of sedimentembedded bridge piers. *Experiments in Fluids* **42**: 1–19.

